

UCLA

UCLA Previously Published Works

Title

Intracapillary LPL levels in brown adipose tissue, visualized with an antibody-based approach, are regulated by ANGPTL4 at thermoneutral temperatures.

Permalink

<https://escholarship.org/uc/item/9kw4v0cj>

Journal

Proceedings of the National Academy of Sciences of USA, 120(8)

Authors

Song, Wenxin
Yang, Ye
Heizer, Patrick
[et al.](#)

Publication Date

2023-02-21

DOI

10.1073/pnas.2219833120

Peer reviewed



Intracapillary LPL levels in brown adipose tissue, visualized with an antibody-based approach, are regulated by ANGPTL4 at thermoneutral temperatures

Wenxin Song^a, Ye Yang^a, Patrick Heizer^a, Yiping Tu^a, Thomas A. Weston^a, Joonyoung R. Kim^a, Priscilla Munguia^a, Hyesoo Jung^a, Jared L.-C. Fong^a, Caitlyn Tran^a, Michael Ploug^{b,c}, Anne P. Beigneux^a, Stephen G. Young^{a,d,1}, and Loren G. Fong^{a,1}

Contributed by Stephen G. Young; received December 7, 2022; accepted January 18, 2023; reviewed by Pao-Tien Chuang and Renate Schreiber

Lipoprotein lipase (LPL) is secreted into the interstitial spaces by parenchymal cells and then transported into capillaries by GPIHBP1. LPL carries out the lipolytic processing of triglyceride (TG)-rich lipoproteins (TRLs), but the tissue-specific regulation of LPL is incompletely understood. Plasma levels of TG hydrolase activity after heparin injection are often used to draw inferences about intravascular LPL levels, but the validity of these inferences is unclear. Moreover, plasma TG hydrolase activity levels are not helpful for understanding LPL regulation in specific tissues. Here, we sought to elucidate LPL regulation under thermoneutral conditions (30 °C). To pursue this objective, we developed an antibody-based method to quantify (in a direct fashion) LPL levels inside capillaries. At 30 °C, intracapillary LPL levels fell sharply in brown adipose tissue (BAT) but not heart. The reduced intracapillary LPL levels were accompanied by reduced margination of TRLs along capillaries. ANGPTL4 expression in BAT increased fourfold at 30 °C, suggesting a potential explanation for the lower intracapillary LPL levels. Consistent with that idea, *Angptl4* deficiency normalized both LPL levels and TRL margination in BAT at 30 °C. In *Gpihbp1*^{-/-} mice housed at 30 °C, we observed an ANGPTL4-dependent decrease in LPL levels within the interstitial spaces of BAT, providing in vivo proof that ANGPTL4 regulates LPL levels before LPL transport into capillaries. In conclusion, our studies have illuminated intracapillary LPL regulation under thermoneutral conditions. Our approaches will be useful for defining the impact of genetic variation and metabolic disease on intracapillary LPL levels and TRL processing.

triglyceride hydrolysis | intravascular lipolysis | brown adipose tissue | ANGPTL4 | thermoneutral

Lipoprotein lipase (LPL) is synthesized by parenchymal cells (e.g., adipocytes, myocytes) and secreted into the interstitial spaces, where it is captured by a plasma membrane-anchored protein of capillary endothelial cells (ECs), glycosylphosphatidylinositol-anchored high-density lipoprotein-binding protein 1 (GPIHBP1) (1). GPIHBP1 shuttles LPL across ECs to the capillary lumen (2). When GPIHBP1 is absent, LPL remains trapped within the interstitial spaces and does not reach the luminal surface of ECs (2). The importance of LPL and GPIHBP1 for plasma triglyceride (TG) metabolism is evident by the fact that a deficiency in either protein causes severe hypertriglyceridemia (chylomicronemia) (3–6).

LPL and the processing of TG-rich lipoproteins (TRLs) are regulated in a tissue-specific manner by angiopoietin-like (ANGPTL) proteins (7). For example, LPL-mediated TRL processing in white adipose tissue (WAT) is reduced during fasting, largely due to inhibition of LPL by ANGPTL4 (8). ANGPTL4 inactivates LPL by catalyzing the unfolding of LPL's aminoterminal TG hydrolase domain (9–12). In contrast, LPL-mediated TRL processing in striated muscle is reduced after feeding, largely due to increased LPL inhibition by ANGPTL3/8 (13–15).

TRL processing is also regulated by ambient temperature. When mice are housed at 4 °C, core body temperature is maintained by the activation of nonshivering thermogenesis in brown adipose tissue (BAT), a process that is mediated by uncoupling protein 1 (UCP1) (16). The induction of thermogenesis at 4 °C is accompanied by increased TRL processing and fatty acid oxidation. When mice are housed at 4 °C, the uptake of TRL-derived lipids by BAT is increased and plasma TG levels fall (17). In *Apoa5*^{-/-} mice where plasma TG levels are elevated, exposure to the cold normalizes plasma TG levels (17). The impact of the cold on LPL levels inside capillaries has never been examined, but an important role for intravascular LPL in TRL processing in BAT was inferred because a nonspecific lipase inhibitor impeded TRL processing and because lipid uptake was reduced by heparin (the presumption was that heparin had depleted intravascular LPL levels in BAT) (17). ANGPTL4 is important for regulating LPL activity during cold exposure (18). LPL activity in BAT markedly increases in wild-type (WT) mice upon prolonged cold-exposure

Significance

Lipoprotein lipase (LPL), an intravascular triglyceride hydrolase, is crucial for plasma triglyceride metabolism, and genetic variation that reduces LPL-mediated triglyceride hydrolysis increases the risk of coronary heart disease. Intravascular LPL levels are frequently inferred from measurements of triglyceride hydrolase activity in the plasma after a bolus of heparin, but whether such measurements truly reflect intravascular LPL levels has been unclear. We developed a direct, antibody-based method to both visualize and quantify intravascular LPL levels. We discovered that LPL levels in capillaries fall sharply in brown adipose tissue (but not heart) under thermoneutral conditions, due to increased ANGPTL4 expression. Our methods can be applied to define the impact of genetic variation, hypolipidemic drugs, and metabolic diseases on intravascular LPL levels.

Reviewers: P.-T.C., University of California; and R.S., Karl-Franzens-Universität Graz.

The authors declare no competing interest.

Copyright © 2023 the Author(s). Published by PNAS. This article is distributed under [Creative Commons Attribution-NonCommercial-NoDerivatives License 4.0 \(CC BY-NC-ND\)](https://creativecommons.org/licenses/by-nc-nd/4.0/).

¹To whom correspondence may be addressed. Email: syoung@mednet.ucla.edu or lfong@mednet.ucla.edu.

This article contains supporting information online at <https://www.pnas.org/lookup/suppl/doi:10.1073/pnas.2219833120/-/DCSupplemental>.

Published February 14, 2023.

and this is attenuated in *Angptl4* transgenic mice (18). Housing mice at temperatures within their thermoneutral zone (i.e., 29 to 31 °C) (19) reduces the activation of thermogenesis in BAT and reduces the uptake of lipids from chylomicrons (20). LPL activity is reduced in BAT at thermoneutral temperatures (when compared with mice exposed to the cold), but total LPL protein levels in BAT appear to be higher at thermoneutral temperatures than in the cold (18). The impact of thermoneutral conditions on LPL levels within BAT capillaries has never been examined.

For years, the regulation of LPL and intravascular TRL processing has been studied with indirect methods. Intravascular LPL levels have been inferred from LPL levels in tissue extracts, measuring levels of TG hydrolase activity in the postheparin plasma, measuring the uptake of radioactive lipids by tissues, and measuring transcripts for LPL and/or physiologic regulators of LPL (e.g., ANGPTL4, ANGPTL3, ANGPTL8). Whether any of these approaches accurately reflect intravascular LPL levels has never been tested.

In the current study, we developed an antibody-based method to visualize and quantify intracapillary LPL levels and used that method to investigate LPL regulation in mouse tissues. Specifically, we investigated whether thermoneutral conditions reduce intracapillary LPL levels, and if so, whether reduced intracapillary LPL levels are accompanied by reduced TRL margination along

capillaries. We also studied the impact of thermoneutrality on LPL levels in *Gpiihbp1*^{-/-} mice, where LPL is trapped in the interstitial spaces and never reaches the capillary lumen (2).

Results

Housing Mice at 30 °C Reduces Plasma TG Metabolism. We sought to understand the effect of thermoneutrality on LPL expression and TRL margination in BAT capillaries. As expected, housing mice at 30 °C reduced *Ucp1* transcripts in BAT by ~80% and UCP1 protein levels by ~50% (Fig. 1 *A* and *B*); lipid droplet size in brown adipocytes increased from 4 to 46 μm^2 (Fig. 1 *C* and *D* and *SI Appendix, Fig. S1A*); and the expression of multiple genes related to lipid metabolism was perturbed (*SI Appendix, Fig. S1B*). Plasma TG levels increased in both male and female mice at 30 °C (*SI Appendix, Fig. S1C*). When male and female mice were pooled, the mean plasma TG level increased by ~75% (from 50 to 88 mg/dL; $P < 0.001$) (Fig. 1*E*). Amounts of LPL activity in the plasma after an intravenous bolus of heparin were ~20% lower in mice housed at 30 °C than at room temperature (RT) ($P < 0.01$) (Fig. 1*F*). LPL mass levels in the postheparin plasma trended lower at 30 °C, but the difference was not statistically significant ($P = 0.22$) (Fig. 1*G*). Because the LPL in postheparin plasma is

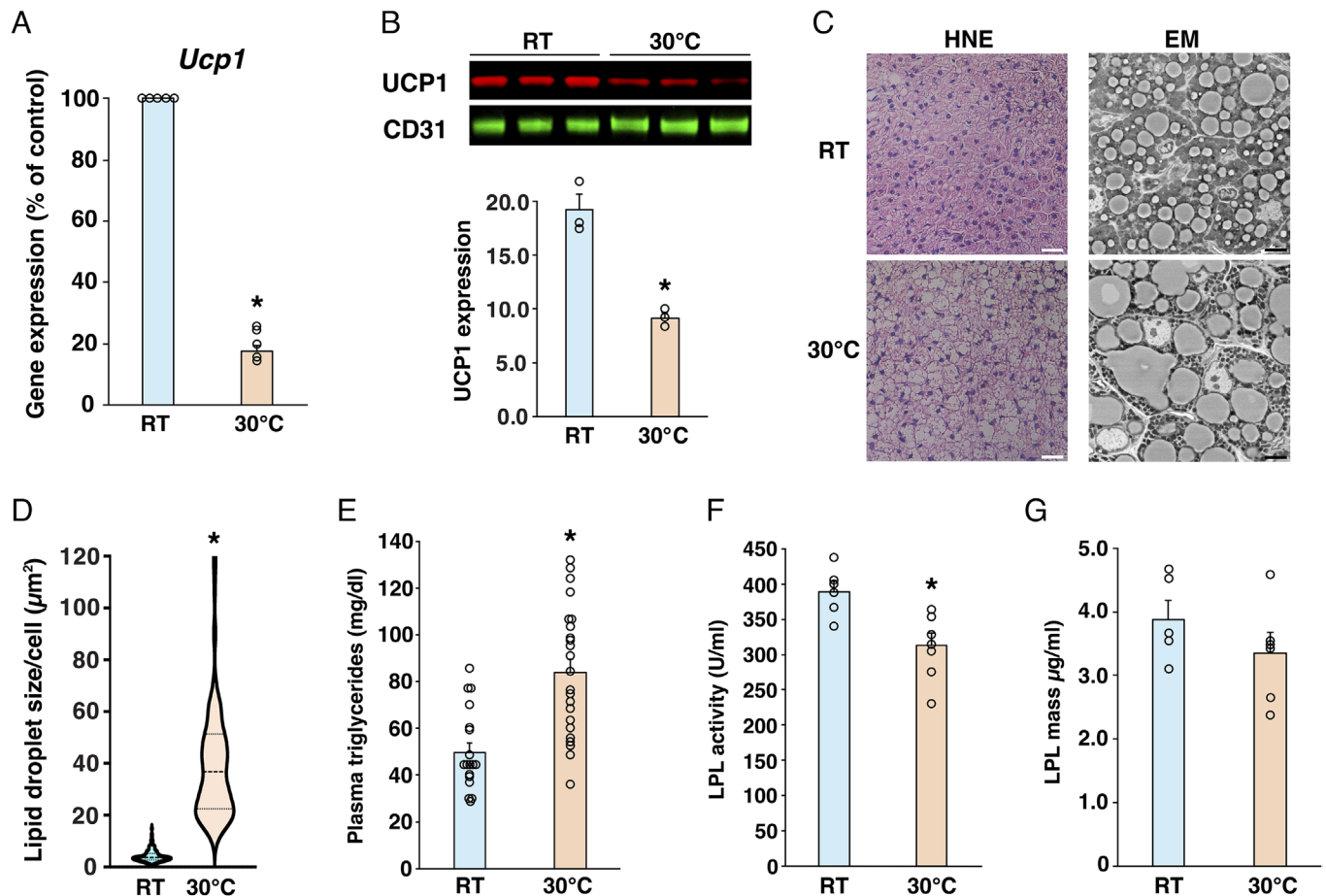


Fig. 1. Housing mice at 30 °C reduces plasma TG metabolism. (A) *Ucp1* expression in BAT from mice housed at 30 °C or RT in five experiments. Mean \pm SEM. $*P < 0.001$. (B) Western blot studies showing reduced UCP1 protein levels in BAT from mice housed at 30 °C. (Upper) Western blot of UCP1 and CD31. Each lane represents an individual mouse. (Lower) Bar graph showing reduced UCP1 levels (relative to CD31) in mice at 30 °C. Mean \pm SEM. $*P < 0.01$. (C) Representative hematoxylin and eosin (HNE)-stained sections (Left) and EM micrographs (Right) of BAT from mice housed at RT or 30 °C. [Scale bar, 25 μm (HNE). Scale bar, 5 μm (EM).] (D) Violin plots showing that lipid droplet size in BAT is increased at 30 °C. A minimum of 130 cells were analyzed/group. Mean \pm SEM. $*P < 0.001$. (E) Bar graph showing that plasma TGs were higher in mice housed at 30 °C ($n = 23$) than in mice at RT ($n = 18$ mice). Mean \pm SEM. $*P < 0.001$. Levels for male and female mice were pooled. Plasma TG levels separated by sex are shown in *SI Appendix, Fig. S1C*. (F) LPL activity in the postheparin plasma from mice housed at 30 °C is lower than in mice housed at RT (6 to 7 mice/group). Mean \pm SEM. $*P < 0.01$. (G) LPL mass levels in the postheparin plasma from mice housed at RT or 30 °C (5 to 6 mice/group) are not statistically different ($P = 0.274$). Mean \pm SEM.

derived from multiple tissues, we could not draw any inferences about LPL levels in BAT.

Detecting LPL in Mice with a Monospecific Antibody. We purified mouse LPL from *Sf9* cells (21) and used it to generate a rabbit polyclonal antibody against mouse LPL (Ab3174) (22). The antibody was useful for immunoprecipitating unbound LPL and GPIHBP1-bound LPL (Fig. 2A and B). To assess whether Ab3174

is capable of detecting LPL along the luminal surface of ECs, we gave an intravenous injection of Ab3174 and a CD31-specific monoclonal antibody (2H8) to WT mice and to *Lpl^{-/-}* mice that expressed human LPL in ECs (*Lpl^{-/-}Tie2-LPL*). After 2 min, the vasculature was perfused with PBS, and tissue sections were stained with species-specific fluorescent secondary antibodies. Ab3174 bound avidly to the luminal surface of capillaries in WT mice, but there was no binding of Ab3174 in *Lpl^{-/-}Tie2-LPL* mice (Fig. 2C). In

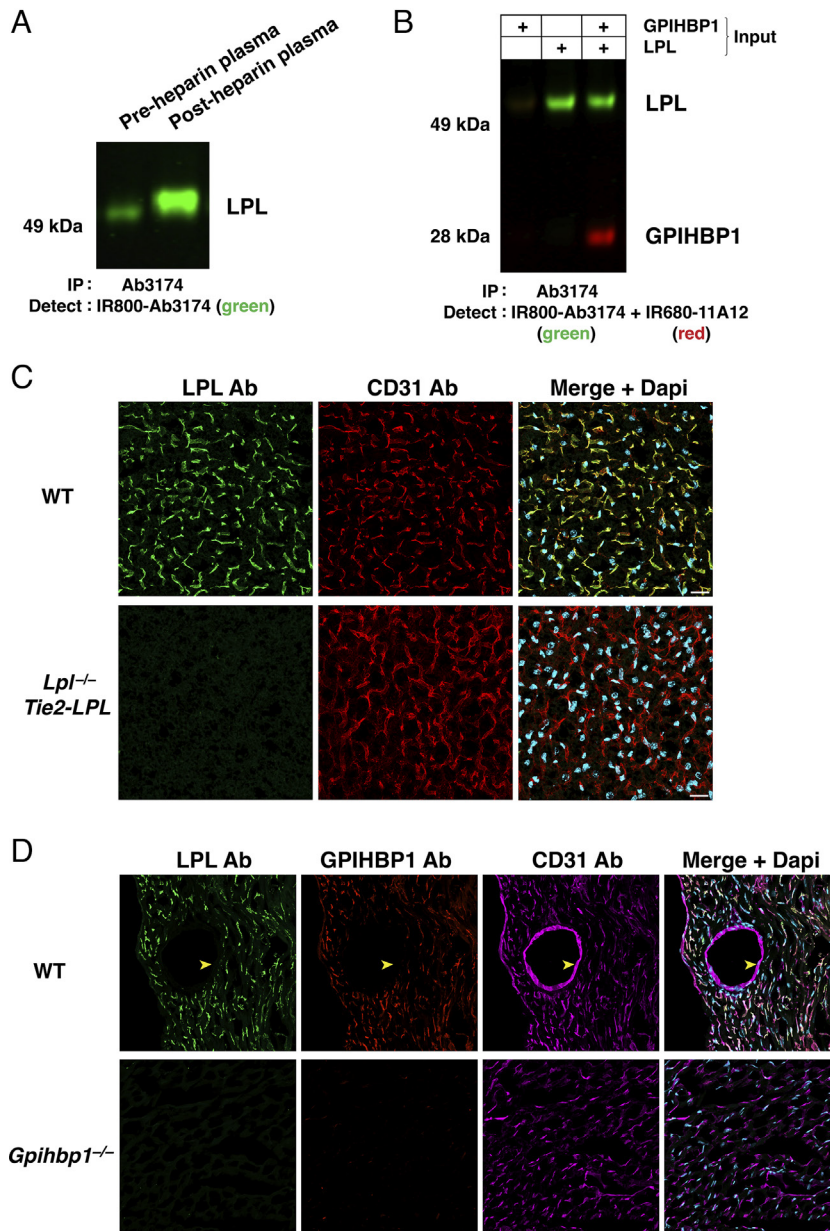


Fig. 2. Detecting LPL in mice with a monospecific antibody. (A) Western blot showing that Ab3174 can capture LPL in preheparin and postheparin plasma. Preheparin and postheparin plasma samples were incubated with magnetic beads coated with Ab3174. The immune precipitates were analyzed by western blotting with IRDye800-labeled Ab3174 (green). (B) Western blot showing that Ab3174 can bind to free and GPIHBP1-bound LPL. Recombinant mouse LPL, recombinant mouse GPIHBP1, or LPL-GPIHBP1 complexes were incubated with magnetic beads coated with Ab3174. The immune precipitates were analyzed by western blotting with IRDye800-Ab3174 (green) and IRDye680-11A12 (red). (C) Confocal microscopy images showing that Ab3174 can detect intravascular LPL in BAT of WT mice but not *Lpl^{-/-}Tie2-LPL* mice. Mice were injected intravenously with antibodies against LPL (Ab3174) and CD31 (2H8); after 2 min, the vasculature was perfused with PBS, followed by fixative. Tissue sections of BAT were stained with species-specific fluorescent-labeled antibodies. Representative confocal microscopy images show robust binding of Ab3174 (green) to capillaries of WT mice but not *Lpl^{-/-}Tie2-LPL* mice; the binding of 2H8 (red) was similar in both mouse strains. Nuclei were stained with Dapi (blue). (Scale bar, 20 μ m.) (D) Confocal microscopy images showing that Ab3174 detects intravascular LPL in the heart of WT mice but not *Gpihbp1^{-/-}* mice. Mice were injected intravenously with antibodies against LPL (Ab3174), CD31 (2H8), and GPIHBP1 (11A12); after 2 min, the vasculature was perfused with PBS, followed by fixative. Tissue sections of heart were processed for confocal fluorescence microscopy. Images show robust binding of Ab3174 (green) to capillaries in the heart of WT mice but negligible binding in *Gpihbp1^{-/-}* mice. Ab3174 binding to the large blood vessel was absent (yellow arrowhead). The binding of 2H8 (magenta) was similar in both mouse strains; 11A12 binding (red) was absent in *Gpihbp1^{-/-}* mice. Nuclei were stained with Dapi (blue). (Scale bar, 20 μ m.)

Gpiihbp1^{-/-} mice, where LPL transport into capillaries is negligible, Ab3174 binding to capillaries was essentially absent (Fig. 2D).

LPL Levels in BAT Are Reduced at 30 °C. We examined, by immunofluorescence confocal microscopy, the binding of Ab3174 to tissue sections of mice housed at 30 °C or RT. LPL staining in BAT was lower in mice housed at 30 °C than at RT (Fig. 3A and *SI Appendix, Fig. S2A*), but amounts of LPL in heart and quadriceps were similar at 30 °C and RT (*SI Appendix, Fig. S2 B and C*). The less intense LPL staining in BAT at 30 °C was largely due to reduced staining in GPIHBP1- and CD31-positive capillary ECs (Fig. 3A). GPIHBP1 or CD31 expression was not perturbed at 30 °C. Western blots of BAT extracts yielded consistent results; amounts of LPL in BAT were lower at 30 °C than at RT ($P < 0.001$; 7 mice/group) (*SI Appendix, Fig. 3 B and C*).

Reduced Amounts of LPL on the Luminal Surface of BAT Capillaries at 30 °C. To assess the impact of thermoneutrality on amounts of LPL inside capillaries, we gave mice an intravenous

injection of antibodies against LPL (Ab3174), GPIHBP1 (11A12), and CD31 (2H8). Ab3174 binding to the luminal surface of BAT capillaries (relative to either 11A12 or 2H8) was lower at 30 °C than at RT (Fig. 4A); the binding of 11A12 and 2H8 to BAT capillaries was similar at 30 °C and RT.

To assess intracapillary LPL levels with a more quantitative method, we gave mice an intravenous injection of infrared dye (IRDye)-labeled antibodies (IR680-Ab3174, IR800-11A12). After 2 min, the vasculature was perfused with PBS; tissue sections were prepared; and antibody binding to tissue sections was quantified with an infrared scanner. Ab3174 binding, relative to 11A12, was substantially reduced at 30 °C in BAT (Fig. 4B and *SI Appendix, Fig. S3A*) but not in heart (Fig. 4B). Quantification of IRDye signals revealed that intracapillary LPL levels in BAT at 30 °C were reduced by 65% (Fig. 4B and *SI Appendix, Fig. S3B*).

To determine if the lower amounts of LPL in BAT capillaries at 30 °C resulted in reduced TRL margination within capillaries, we gave mice an intravenous injection of a lipase inhibitor (to block TG hydrolysis), IRDye680-labeled TRLs, and IRDye800-2H8. After

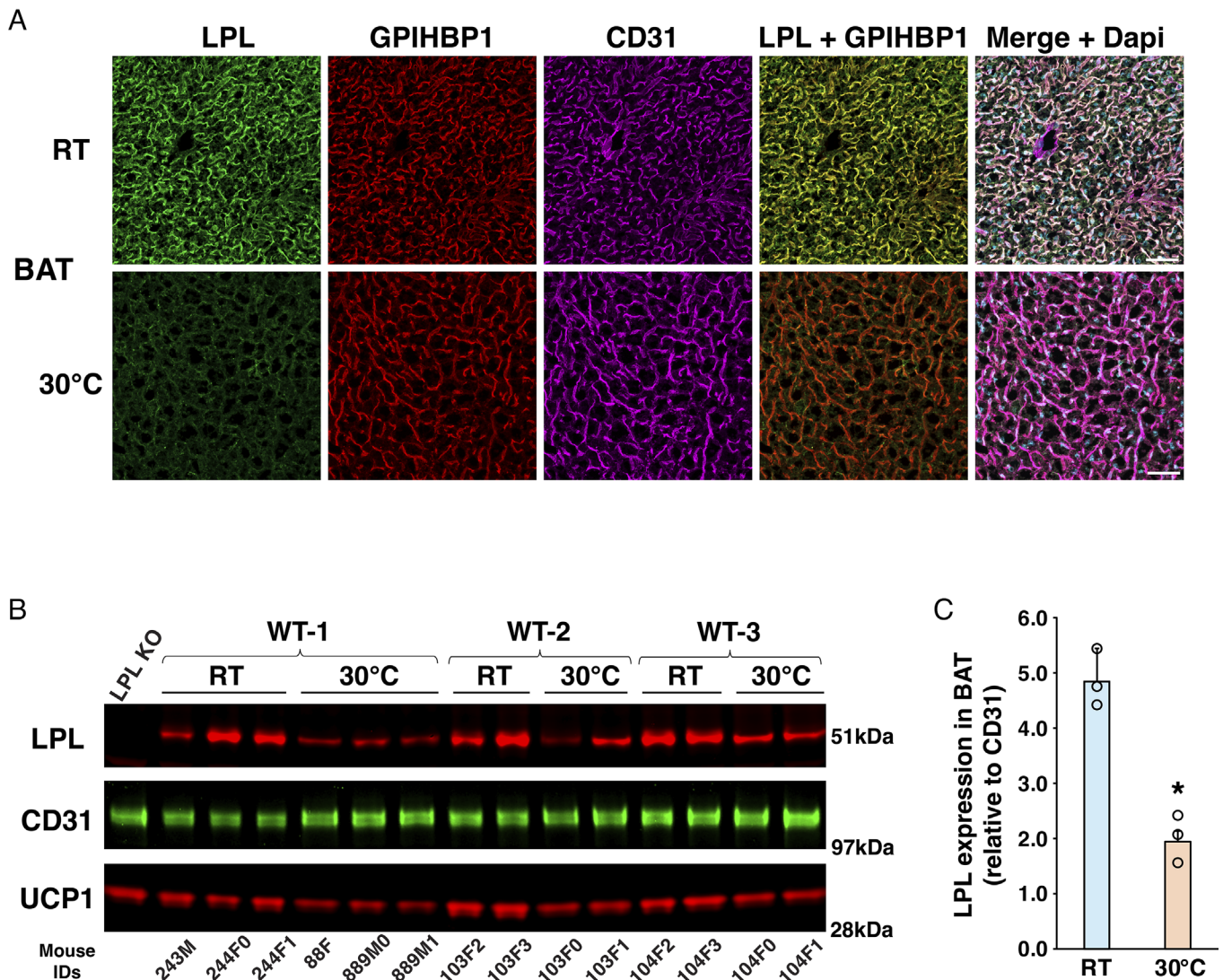


Fig. 3. LPL levels in BAT are reduced at 30 °C. (A) Confocal fluorescence microscopy images showing that LPL levels in BAT are reduced in mice housed at 30 °C. Tissue sections of BAT from mice housed at 30 °C or RT were processed for indirect immunofluorescence microscopy with antibodies against LPL (green), GPIHBP1 (red), and CD31 (magenta). Nuclei were stained with Dapi (blue). (Scale bar, 50 μ m.) (B) Western blot studies showing LPL levels in BAT are lower in mice housed at 30 °C than at RT. Blots were performed with antibodies against LPL (Ab3174), CD31 (goat polyclonal), and UCP1 (rabbit polyclonal). Each lane represents an individual mouse from three experiments (WT-1, WT-2, and WT-3). Note that UCP1 levels are lower in BAT extracts from mice housed at 30 °C. (C) Bar graph showing reduced LPL levels in BAT from mice housed at 30 °C. LPL expression, relative to CD31, was quantified in the three experiments shown in panel B. Mean \pm SEM. * $P < 0.001$.

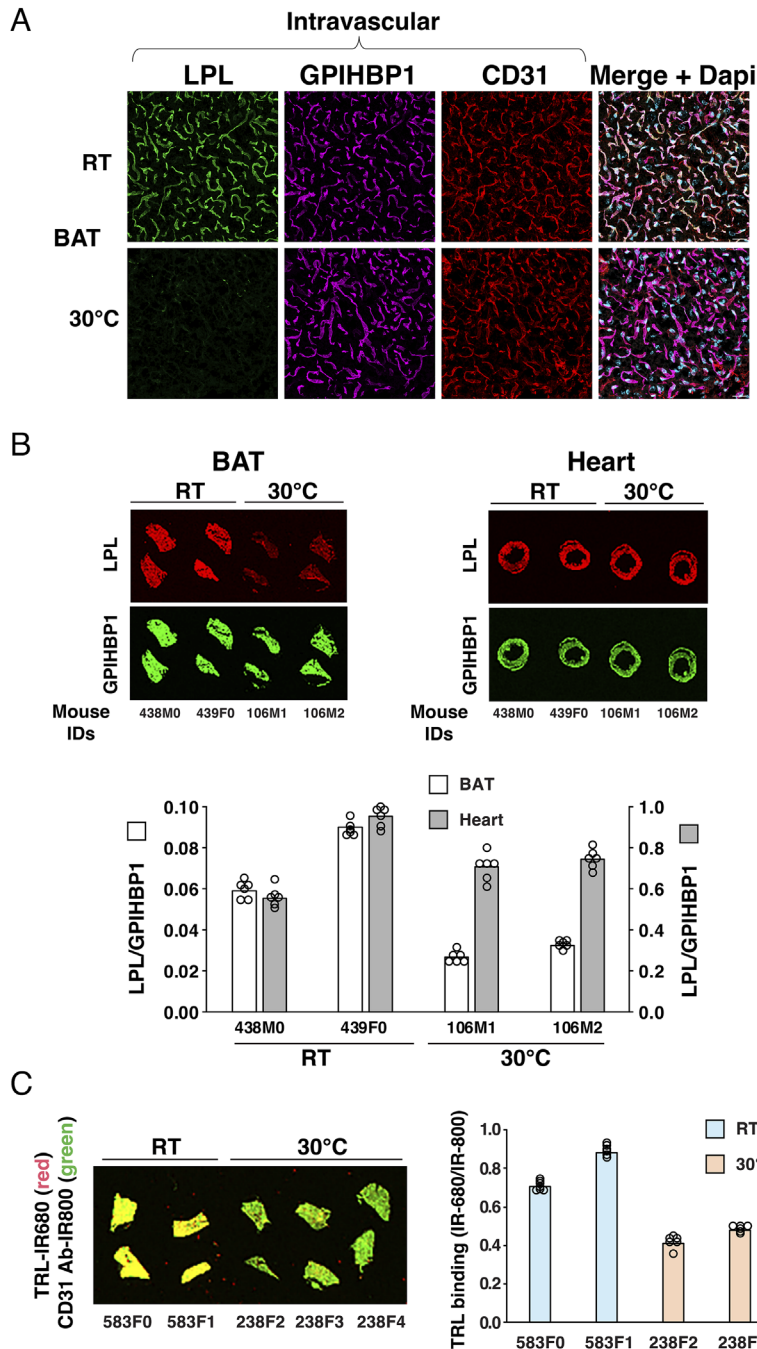


Fig. 4. Reduced amounts of LPL on the luminal surface of BAT capillaries at 30 °C. (A) Fluorescence microscopy images showing binding of antibodies Ab3174 (green), 11A12 (magenta), and 2H8 (red) in BAT after an intravenous injection of those antibodies into mice housed at RT or 30 °C. (Scale bar, 20 μm.) (B) (Upper) Representative infrared scans of tissue sections showing the binding of IRDye680-Ab3174 (red) and IRDye800-11A12 (green) in BAT and heart of mice housed at RT or 30 °C. Each column represents an individual mouse. (Lower) Bar graph showing the binding of the IRDye680-Ab3174 antibody, relative to the IRDye800-11A12, in BAT (white) and heart (gray) sections (6 sections/tissue). (C) (Left) Representative infrared scans of BAT tissue sections following an intravenous injection of IRDye680-labeled TRLs (red) and IRDye800-2H8 (green) into mice housed at RT or at 30 °C. Each column represents an individual mouse. Yellow color represents strong binding of both TRLs and 2H8. Green color represents reduced amounts of TRL binding. (Right) Bar graph showing the binding of IRDye680-TRLs (relative to IRDye800-2H8) at RT (blue) and 30 °C (tan) in BAT sections (6 sections/tissue).

perfusing the vasculature with PBS and preparing tissue sections, amounts of TRL margination in BAT, relative to 2H8 binding, was assessed with an infrared scanner. TRL margination was 47% lower at 30 °C than at RT (Fig. 4C and *SI Appendix, Fig. S3 C and D*).

Thermoneutrality Does Not Reduce GPIHBP1 Expression nor Does It Disrupt GPIHBP1 Trafficking Across ECs. GPIHBP1 levels in BAT extracts were assessed by western blotting (Fig. 5A). Quantification of blots revealed that amounts of GPIHBP1, relative to CD31, were similar in BAT at 30 °C and RT

($P = 0.97$; 7 mice/group) (Fig. 5B). That finding was consistent with our microscopy studies (Figs. 3A and 4A).

To determine if thermoneutral conditions influenced GPIHBP1 trafficking across ECs in BAT, we began using confocal microscopy to compare amounts of GPIHBP1 on the abluminal and luminal surfaces of capillary ECs (2, 23) (Fig. 5C). GPIHBP1 was distributed equally between the luminal and abluminal surfaces of ECs at both 30 °C and RT (Fig. 5D), implying that GPIHBP1 trafficking was probably not affected by ambient temperature. To assess GPIHBP1 trafficking in a direct fashion, we injected Alexa

Fluor 555–11A12 and Alexa Fluor 488–tomato lectin into BAT pads (22). After 90 min, we assessed, by fluorescence microscopy, GPIHBP1-mediated 11A12 transport from the abluminal to the

luminal surface of BAT capillaries (Fig. 5E). These studies revealed that GPIHBP1 trafficking across ECs was similar in mice housed at 30 °C or RT (Fig. 5F).

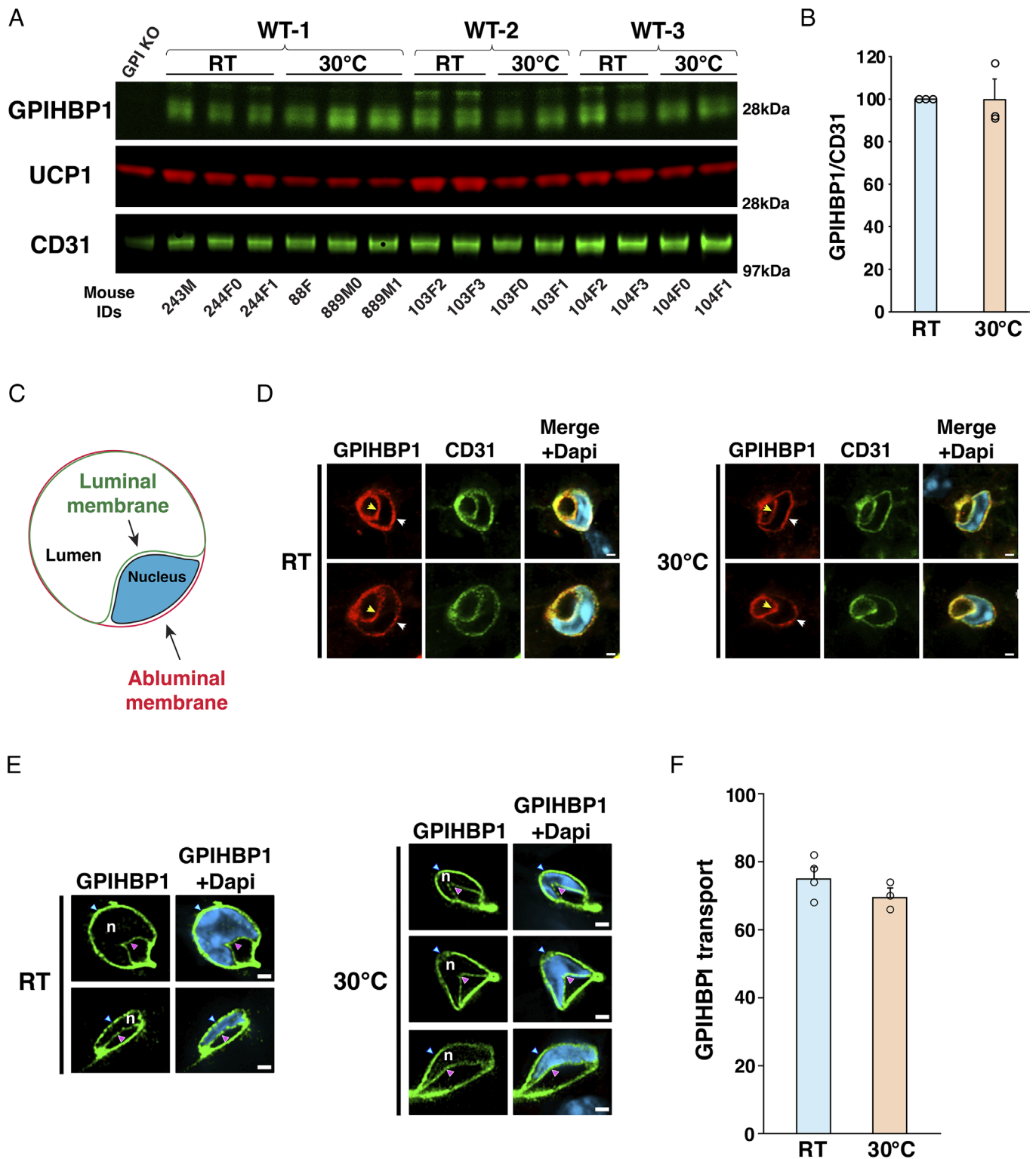


Fig. 5. Thermoneutrality does not reduce GPIHBP1 expression nor does it disrupt GPIHBP1 trafficking across ECs. (A) Western blots showing that GPIHBP1 levels in BAT are not reduced at 30 °C. Each lane represents an individual mouse from three experiments (WT-1, WT-2, and WT-3). (B) Quantification of GPIHBP1 bands in panel A (relative to CD31). Mean \pm SEM ($n = 3$ experiments; $P = 0.97$). (C) Schematic of a capillary cross-section, depicting the separation of the abluminal plasma membrane (APM; red) and luminal plasma membranes (LPM; green) by an EC nucleus. (D) Representative confocal micrographs of BAT capillary cross-sections showing that the distributions of GPIHBP1 (red) along the LPM (yellow arrow) and APM (white arrow) are similar at RT and 30 °C. (Scale bar, 1 μ m.) (E) Representative images of capillary cross-sections containing an EC nucleus (n; blue), revealing the distribution of GPIHBP1 (green) along the LPM (red arrowhead) and the APM (blue arrowhead) following an injection of Alexa Fluor 555–11A12 and Alexa Fluor-488–tomato lectin into BAT pads of mice. (Scale bar, 1 μ m.) (F) Quantification of capillary cross-sections (from a total of 50 counted) in which Alexa Fluor 555–11A12 was observed in the capillary lumen. Mean \pm SEM. $P = 0.23$ (3 mice/group).

Increased *Angptl4* Expression at 30 °C Is Responsible for the Reduced Amounts of LPL in BAT. Finding reduced amounts of LPL in BAT but not in the heart or skeletal muscle (SI Appendix, Fig. S2) suggested that LPL was subject to local regulation in BAT. We measured *Lpl* transcript levels in BAT at 30 °C, along with transcripts for genes that regulate LPL. At 30 °C, *Lpl* transcripts were reduced by 23% ($P < 0.05$), whereas *Angptl4* expression increased ~fourfold ($P < 0.01$) (Fig. 6A). *Angptl3* and *Angptl8* expression were similar at RT and 30 °C.

We suspected that increased *Angptl4* expression and decreased *Lpl* expression contributed to the reduced levels of LPL in BAT at 30 °C, but we wanted to exclude the possibility that the reduced *Lpl* transcripts contributed disproportionately. We therefore examined LPL expression in BAT of *Lpl*^{-/-} mice, where *Lpl* transcripts are reduced by ~50% and *Angptl4* transcripts are not perturbed (Fig. 6B). The intensity of LPL staining in BAT of *Lpl*^{-/-} mice at RT was far greater than in WT mice housed at 30 °C (Fig. 6C), implying that increased *Angptl4* expression in BAT at 30 °C is largely responsible for the reduced amounts of LPL in

capillaries. Similar results were observed in independent groups of mice (SI Appendix, Fig. S4).

***Angptl4* Deficiency Normalizes LPL Levels and TRL Margination in BAT at 30 °C.** Housing *Angptl4*^{-/-} mice at 30 °C reduced *Ucp1* expression in BAT and increased the size of lipid droplets in brown adipocytes (SI Appendix, Fig. S5)—similar to findings in WT mice (Fig. 1). However, in contrast to WT mice, where thermoneutrality sharply reduced amounts of LPL levels in BAT, we observed robust amounts of LPL in the BAT of *Angptl4*^{-/-} mice (Fig. 7A). Western blots confirmed that LPL levels in *Angptl4*^{-/-} mice were not reduced at 30 °C (Fig. 7B and C). Also, the binding of Ab3174 to the luminal surface of capillaries, relative to 11A12 and 2H8, was similar in *Angptl4*^{-/-} mice at RT or 30 °C (Fig. 7D). The preserved intracapillary LPL levels in BAT of *Angptl4*^{-/-} mice at 30 °C suggested that TRL margination along BAT capillaries would be greater in *Angptl4*^{-/-} mice than in WT mice. Indeed, this was the case (Fig. 7E and F).

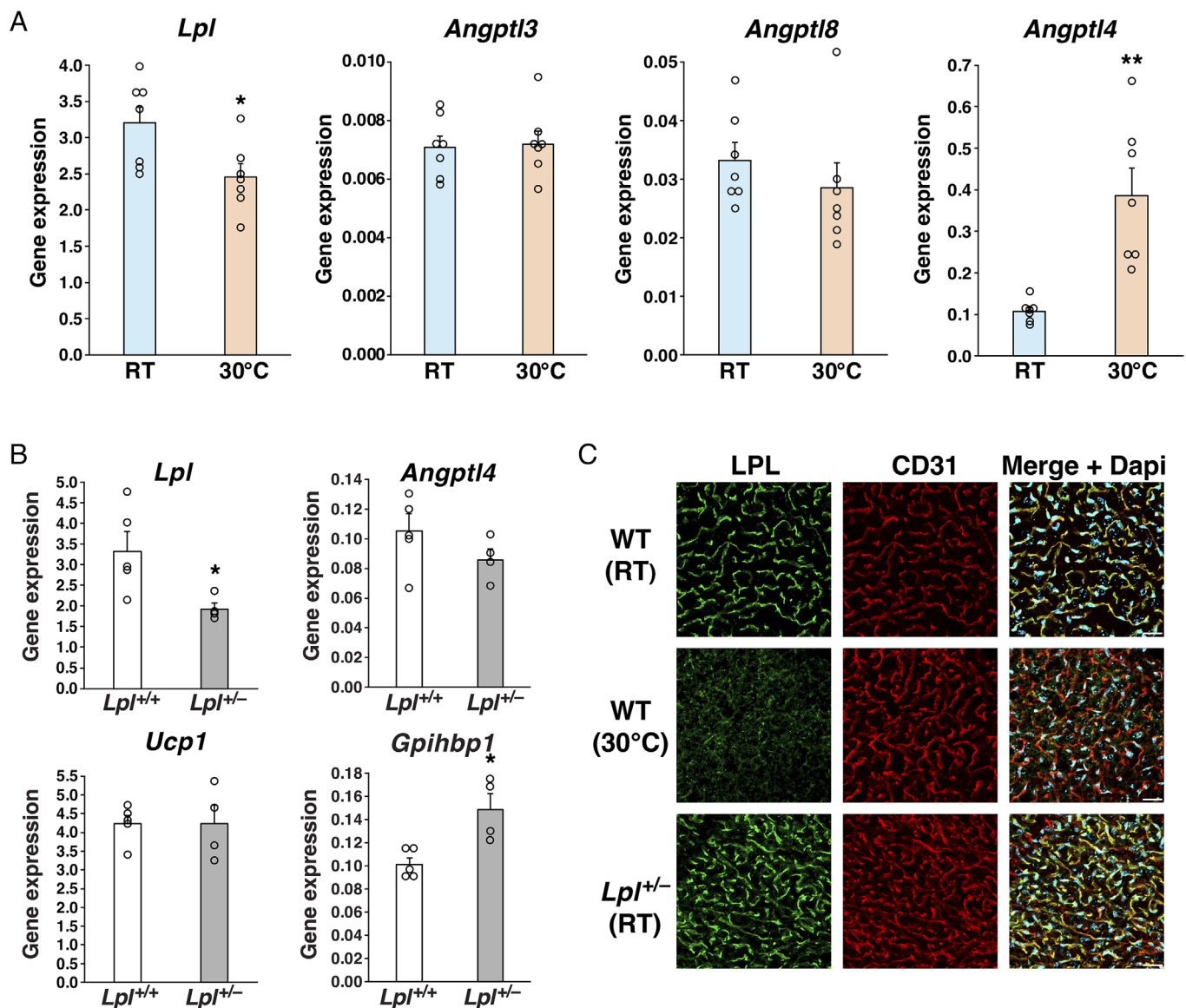


Fig. 6. Increased *Angptl4* expression at 30 °C is responsible for the decreased amounts of LPL in BAT. (A) Expression of *Lpl*, *Angptl3*, *Angptl8*, and *Angptl4* in BAT from WT mice housed at RT ($n = 12$ mice) or 30 °C ($n = 14$ mice) in seven experiments. Mean \pm SEM. * $P < 0.05$, ** $P < 0.01$. (B) Expression of *Lpl*, *Angptl4*, *Ucp1*, and *Gpihbp1* in BAT from *Lpl*^{+/+} ($n = 5$) and *Lpl*^{-/-} mice ($n = 4$) housed at RT. Mean \pm SEM. * $P < 0.05$. (C) Representative fluorescence microscopy images of LPL (green) and CD31 (red) in BAT from WT mice housed at RT or 30 °C and *Lpl*^{-/-} mice housed at RT. Nuclei were stained with Dapi (blue). (Scale bar, 20 μ m.)

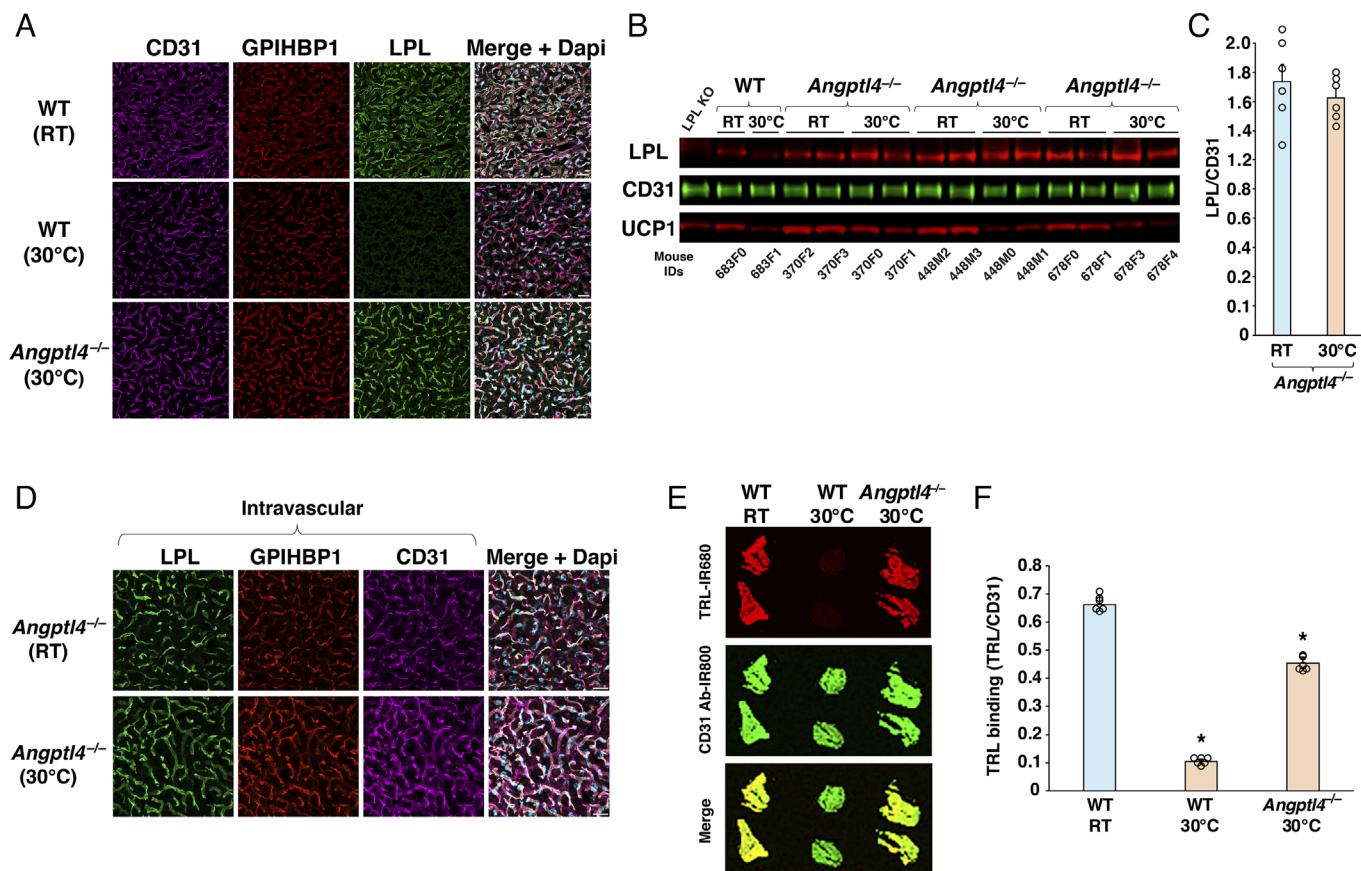


Fig. 7. *Angptl4* deficiency normalizes LPL levels and TRL margination in BAT at 30 °C. (A) Representative fluorescence microscopy images of CD31 (magenta), GPIHBP1 (red), and LPL (green) staining in BAT from WT mice housed at RT or 30 °C and *Angptl4*^{-/-} mice housed at 30 °C. Nuclei were stained with Dapi (blue). (Scale bar, 20 μm.) (B) Western blots of LPL, CD31, and UCP1 in BAT extracts from WT and *Angptl4*^{-/-} mice housed at RT and 30 °C. Each lane represents an individual mouse. (C) Bar graph showing that LPL levels in BAT (assessed by western blotting) do not fall at 30 °C. LPL levels were normalized to CD31 ($n = 6$ mice/group). Mean \pm SEM ($P = 0.45$). (D) Representative fluorescence microscopy images showing that ANGPTL4 deficiency prevents the loss of intravascular LPL in BAT at 30 °C. The binding of LPL (green), GPIHBP1 (red), and CD31 (magenta) antibodies in BAT was examined in *Angptl4*^{-/-} mice after an intravenous injection of Ab3174, 11A12, and 2H8. Nuclei were stained with Dapi (blue). (Scale bar, 20 μm.) (E) Representative infrared scans of BAT sections depicting the binding of IRDye680-TRLs (red) and IRDye800-2H8 (green) after intravenous injection into WT mice housed at RT or 30 °C and *Angptl4*^{-/-} mice housed at 30 °C. Each column represents an individual animal. (F) Bar graph depicting TRL binding (normalized to 2H8 binding) in BAT from WT mice housed at RT or 30 °C and *Angptl4*^{-/-} mice housed at 30 °C (6 sections/tissue). Mean \pm SD. * $P < 0.001$.

Lower Levels of LPL Within the Interstitial Spaces of *Gpibbp1*^{-/-} Mice at 30 °C. In WT mice, increased *Angptl4* expression in BAT at 30 °C led to reduced intracapillary LPL levels. In *Gpibbp1*^{-/-} mice, where LPL is trapped within the interstitial spaces, the effect of 30 °C housing was difficult to predict—simply because little is known about the factors that regulate LPL binding within the interstitial spaces. We therefore examined tissue levels of LPL in *Gpibbp1*^{-/-} mice at 30 °C. By routine IHC, amounts of LPL in the interstitial spaces of BAT of *Gpibbp1*^{-/-} mice were far lower at 30 °C than at RT. In contrast, amounts of LPL in the interstitial spaces of the heart were not perturbed at 30 °C (Fig. 8A). To determine whether the reduced levels of interstitial LPL in BAT of *Gpibbp1*^{-/-} mice at 30 °C were secondary to increased ANGPTL4 expression, we examined interstitial LPL levels in *Gpibbp1*^{-/-}*Angptl4*^{-/-} mice at 30 °C. In those mice, interstitial LPL levels in BAT were preserved at 30 °C (Fig. 8B), demonstrating that interstitial LPL levels in BAT of *Gpibbp1*^{-/-} mice at 30 °C are regulated by ANGPTL4.

Discussion

LPL was characterized by Korn in 1955 as an intravascular TG hydrolase that could be released into the plasma with a bolus of heparin (24, 25). The discovery triggered widespread interest because it was clear that LPL played a central role in plasma TG catabolism and in the delivery of lipid nutrients to peripheral

tissues. For years, LPL was thought to be attached to blood vessels, including large blood vessels, by electrostatic interactions with heparan sulfate proteoglycans (HSPGs) (26). Much later, a protein of capillary ECs, GPIHBP1, was shown to capture LPL within the interstitial spaces and move it to the luminal surface of capillaries (2, 27). Electrostatic forces also play an important role in LPL–GPIHBP1 interactions; the binding of LPL to GPIHBP1 is inhibited by high concentrations of heparin (27–29).

For many decades, measuring TG hydrolase levels in postheparin plasma has been the mainstay for studying genetic and environmental factors affecting plasma TG metabolism. However, while those measurements have been helpful for investigating causes of chylomicronemia (3), they are less helpful for investigating tissue-specific regulation of TG metabolism. LPL activity measurements have never been standardized, and the plasma levels of TG hydrolase activity do not permit inferences about intravascular LPL levels in specific tissues. Moreover, there are lingering questions about whether LPL activity measurements accurately reflect amounts of LPL inside capillaries (30). Measurements of LPL mass in the postheparin plasma are subject to the same questions and reservations. In the current study, we created a direct method for measuring intracapillary LPL levels and then to use that method to investigate LPL regulation under thermoneutral conditions. We used an LPL-specific antibody, Ab3174, to visualize and quantify intracapillary LPL levels. When Ab3174 was

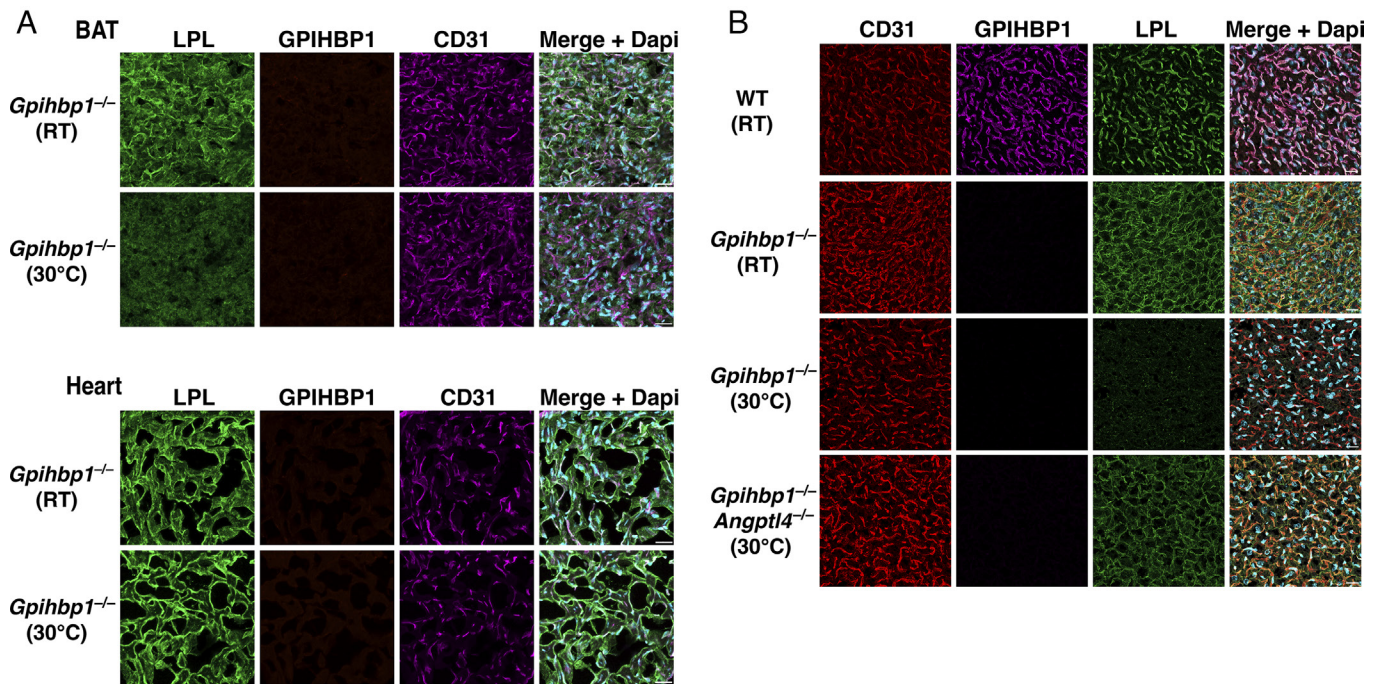


Fig. 8. Lower levels of LPL within the interstitial spaces of *Gpihbp1*^{-/-} mice at 30 °C. (A) Confocal fluorescence microscopy images of LPL (green), CD31 (magenta), and GPIHBP1 (red) in BAT (Upper) and heart (Lower) of *Gpihbp1*^{-/-} mice housed at RT or 30 °C. Nuclei were stained with Dapi (blue). (Scale bar, 20 μm.) (B) Confocal fluorescence microscopy studies of CD31 (red), GPIHBP1 (magenta), and LPL (green) in BAT from WT and *Gpihbp1*^{-/-} mice housed at RT and *Gpihbp1*^{-/-} and *Gpihbp1*^{-/-}*Angptl4*^{-/-} mice housed at 30 °C. Nuclei were stained with Dapi (blue). (Scale bar, 20 μm.)

injected intravenously, it bound to LPL along the luminal surface of capillaries and could be visualized by confocal microscopy and quantified by infrared scanning. Ab3174 binding was specific; there was no binding of Ab3174 to large blood vessels (where GPIHBP1 expression and LPL transport are absent). Furthermore, there was no Ab3174 binding to capillaries of *Gpihbp1*^{-/-} mice (where LPL never reaches the capillary lumen) or to capillaries of *Lpl*^{-/-}*Tie2-LPL* mice.

In WT mice housed at 30 °C, the binding of Ab3174, relative to GPIHBP1- or CD31-specific antibodies, was reduced markedly in capillaries of BAT but not heart. The lower intracapillary LPL levels in BAT were evident both by fluorescence microscopy and infrared scanning. The infrared scanning method is more quantitative and makes it possible to measure antibody binding in a larger tissue area.

In an earlier study (31), we observed markedly reduced TRL margination along capillaries in *Gpihbp1*^{-/-} mice, leading us to propose that TRL margination requires the presence of LPL in capillaries. Our current studies support that proposal. TRL margination in BAT at 30 °C (where intracapillary LPL levels are low) was far lower than at RT (where intracapillary LPL levels are higher). In the heart, TRL margination was not reduced, consistent with preserved intracapillary LPL levels at 30 °C. Our studies are also consistent with the reduced metabolism of radiolabeled TRLs in BAT of mice exposed to thermoneutral temperatures for short periods of time (28 °C for 4 h) (20). The lower intracapillary levels of LPL would reduce not only TRL margination but also the lipolysis of lipoprotein TGs.

We concluded that the reduced intracapillary LPL levels in BAT at 30 °C were largely the result of increased ANGPTL4 expression. Multiple observations supported this conclusion. First, ANGPTL4 is known to down-regulate LPL levels in adipose tissue (8, 18). Second, hydrogen–deuterium exchange/mass spectrometry studies revealed that the binding of ANGPTL4 to LPL lowers the thermal stability of LPLs N-terminal hydrolase domain, thereby triggering

irreversible unfolding, collapse of the catalytic pocket, and enzyme inactivation (9–12). Third, expressing ANGPTL4 in LPL-transfected CHO cells reduced LPL levels (as judged by western blots) and eliminated TG hydrolase activity in the cell culture medium (32). In keeping with the latter observation, LPL secretion from WAT explants was greater in *Angptl4*^{-/-} mice than in WT mice (32). Fourth, and most importantly, our current studies revealed that intracapillary LPL levels in BAT are preserved in *Angptl4*^{-/-} mice housed at 30 °C.

We observed 23% lower *Lpl* transcripts in BAT at 30 °C, but this did not contribute substantially to the reduced intracapillary LPL levels. *Lpl* transcripts in *Lpl*^{-/-} mice were reduced by ~50%, but intracapillary LPL levels in BAT of *Lpl*^{-/-} mice housed at RT were far higher than LPL levels in the BAT of WT mice housed at 30 °C. Neither amounts of GPIHBP1 in BAT capillaries nor GPIHBP1 trafficking across ECs was perturbed at 30 °C.

We also tested whether thermoneutrality affected tissue levels of LPL in *Gpihbp1*^{-/-} mice. GPIHBP1 deficiency eliminates LPL transport into capillaries, triggering an accumulation of LPL in the interstitial spaces. Most of that LPL is bound to HSPGs located near the surface of parenchymal cells and on the outer surface of capillary ECs (2, 23). However, while the existence of a large pool of interstitial LPL in *Gpihbp1*^{-/-} mice is quite clear, we have little understanding of the dynamics of that pool. For example, it is unclear whether the interstitial HSPG binding sites are saturated with LPL, and if so, whether amounts of interstitial LPL would change in response to changes in LPL secretion or LPL stability. The fact that thermoneutral conditions trigger increased ANGPTL4 expression in BAT (but not heart) allowed us to address that issue. When *Gpihbp1*^{-/-} mice were housed at 30 °C, interstitial LPL levels were depleted in BAT but preserved in the heart. The depletion of interstitial LPL in BAT did not occur in *Gpihbp1*^{-/-}*Angptl4*^{-/-} double-knockout mice, demonstrating that ANGPTL4 is responsible for reducing the interstitial LPL pool size in *Gpihbp1*^{-/-} mice. The fact that interstitial LPL levels in BAT

are depleted at 30 °C is consistent with cell culture findings suggesting that ANGPTL4 inactivates LPL within the secretory pathway (32) and is accompanied by LPL cleavage by furin (33).

Our studies open opportunities in plasma TG metabolism research. Rather than having to worry about the reliability of postheparin LPL activity measurements and then drawing inferences about intravascular LPL levels, we can now investigate intracapillary LPL levels directly—and do so in multiple tissues. Our approach—quantifying intracapillary levels of LPL relative to levels of GPIHBP1 and/or CD31—will make it possible to investigate the impact of additional genes related to TG metabolism (e.g., *Apoa5*, *Angptl3*, *Angptl8*, *Ndst1*, and *Col18a1*), TG-lowering agents (e.g., fibrates, nicotinic acid, PPAR agonists, and ANGPTL3/8 antibodies), environmental factors (e.g., exercise, circadian clock), and disease (e.g., sepsis, diabetes mellitus, and cancer cachexia) on intravascular LPL levels. Of note, there is no reason to believe that our method will remain dependent on confocal microscopes and infrared scanners. Our approach could be easily adapted to measuring intracapillary LPL levels and LPL distribution by PET (34) and NanoSIMS microscopy (35).

Materials and Methods

Mouse. C57BL6/J mice were purchased from The Jackson Laboratory. *Gpihbp1*^{-/-}, *Angptl4*^{-/-}, *Gpihbp1*^{-/-}*Angptl4*^{-/-}, *Lpl*^{+/-}, and *Lpl*^{+/-}*Tie2*-LPL mice have been described previously (27, 31, 36). Mice were housed in a specific pathogen-free barrier facility with a 12-h light/dark cycle and an ambient temperature of 22 °C. Mice had free access to mouse chow (NIH31) and water. Unless indicated, all studies were performed in 10 to 13-wk-old male and female C57BL6/J WT mice. Mice were sacrificed between 12 PM and 3 PM. For housing at thermoneutral conditions, mice were placed in nonventilated cages in an incubator at 30 °C for 5 d. All studies involving mice were approved by the University of California at Los Angeles' Animal Research Committee.

Immunohistochemistry Studies. To detect GPIHBP1, LPL, and CD31 in mouse tissues, 10- μ m-thick frozen sections were prepared, fixed with 3% paraformaldehyde (PFA), permeabilized with 0.2% Triton X-100 in PBS, and incubated in blocking buffer (PBS containing 0.2% BSA and 5% donkey serum) for 1 h at RT. Sections were incubated with antibodies against GPIHBP1 (rat monoclonal antibody 11A12, 10 μ g/mL), CD31 (hamster monoclonal antibody 2H8, 10 μ g/mL), and LPL (rabbit polyclonal antibody Ab3174, 8 μ g/mL) at 4 °C overnight. Sections were washed three times to remove unbound antibody and then incubated with fluorescently labeled secondary antibodies for 30 min (Alexa Fluor 488-anti-rabbit IgG, Alexa Fluor 568-anti-rat IgG, and Alexa Fluor-647-anti-hamster IgG) (Invitrogen and Jackson ImmunoResearch) all at a 1:200 dilution. After washing, the sections were postfixed with 3% PFA for 5 min, and cell nuclei were stained with DAPI. Images were obtained on LSM800 or LSM980 microscopes (Zeiss) with 20 \times or 63 \times objectives.

Detecting and Quantifying Intravascular LPL by Fluorescence Microscopy and Infrared Scanning. Mice were injected intravenously with Ab3174, 11A12, and/or 2H8 (150 to 200 μ g each in 0.2 mL sterile saline). After 2 min, mice were perfused with 20 mL PBS through the left ventricle, followed by perfusion with 10 mL 3% PFA. The tissues were embedded in optimal cutting temperature (OCT) compound, and tissue sections were processed for immunofluorescence microscopy.

In separate studies, mice were injected intravenously with IRDye680-labeled Ab3174 and IRDye800-labeled 11A12 (100 to 150 μ g each). After 2 min, mice were perfused with PBS; tissues were embedded in OCT; and 10- μ m-thick frozen sections were prepared (6 sections/tissue/mouse) and scanned using an Odyssey infrared scanner (LI-COR). The Ab3174 signal was normalized to the 11A12 signal.

Western Blotting of Tissue Extracts. Mice were anesthetized with isoflurane, and the vasculature was perfused with PBS. Tissues were harvested, flash-frozen in liquid nitrogen, and homogenized on ice in radioimmunoprecipitation assay buffer containing complete EDTA-free protease inhibitor (Roche). Proteins in the tissue extracts were size-fractionated on a 4 to 12% Bis-Tris SDS-polyacrylamide

gel, and the separated proteins were transferred to a nitrocellulose membrane. Western blots were performed with antibodies against UCP1 (1/4,000; Sigma U6382), CD31 (1/1,000; R&D Systems AF3628), GPIHBP1 (5 μ g/mL; 11A12), and LPL (8 μ g/mL; Ab3174). Antibodies were detected with IRDye680- or IRDye800-labeled secondary antibodies (1:10,000); antibody binding was quantified using an Odyssey infrared scanner.

Immunoprecipitation of LPL. Mouse plasma samples (preheparin and postheparin) were incubated with magnetic beads coated with Ab3174. After removing unbound material, the immune precipitates were size-fractionated on a 4 to 12% Bis-Tris SDS-polyacrylamide gel for western blotting. Mouse LPL was detected with IRDye800-Ab3174. In separate studies, we incubated purified mouse LPL, purified mouse GPIHBP1, or LPL-GPIHBP1 complexes with magnetic beads coated with Ab3174. Immune precipitates were analyzed by western blotting with IRDye800-Ab3174 and IRDye680-11A12.

Quantifying TRL Margination. The margination of TRLs in blood vessels was measured as described previously (31). Briefly, TRLs were isolated from the plasma of *Gpihbp1*^{-/-} mice by ultracentrifugation ($d < 1.006$ g/mL). Mice were injected intravenously with IRDye680-TRLs and IRDye800-2H8 in saline containing 0.25 mM tetrahydrolipstatin. After 60 s, mice were perfused with 20 mL PBS through the left ventricle, followed by 10 mL 3% PFA in PBS. Tissues were embedded in OCT; 10- μ m-thick frozen sections were prepared (6 sections/tissue/mouse) and scanned using an infrared scanner. The TRL signal was normalized to the 2H8 signal.

Measuring GPIHBP1 Transport Across Capillary ECs. GPIHBP1 transport across capillary ECs in BAT of living mice (housed at either 22 °C or 30 °C) was examined as described (2, 22, 23). Briefly, a BAT pad was injected with 3 μ g Alexa Fluor 555-11A12, 3 μ L India ink (to visualize the injected area in frozen sections), and 3 μ g Alexa Fluor 488-tomato lectin (to visualize the injected area by fluorescence microscopy). After 90 min, mice were anesthetized and then perfused with 20 mL PBS followed by 10 mL 3% PFA. Tissues were embedded in OCT; 10- μ m-thick frozen sections were prepared; and cell nuclei were stained with DAPI. Confocal micrographs of capillary cross-sections ($n = 50$ /mouse) were used to quantify the efficiency of Alexa Fluor 555-11A12 movement to the capillary lumen.

Gene Expression Measurements. RNA was extracted from flash-frozen tissues with TRI reagent (Molecular Research), and cDNA was prepared with random primers, oligo(dT), and SuperScript III (Invitrogen). Real-time PCR was performed in triplicate using a QuantStudio five Real-Time PCR System from Applied Biosystems with a SYBR Green PCR Master Mix. Gene-expression levels were calculated with the comparative CT method (37). Primer sequences are in [SI Appendix, Table S1](#).

Measurements of Plasma TG Levels, LPL Mass, and TG Hydrolase Activity. TG levels in mouse plasma samples were measured using the Serum TG Determination Kit (Millipore-Sigma). LPL mass and activity were measured in plasma samples (collected 2 min after an intravenous injection of 15 U heparin). The plasma samples were adjusted to 1.2 M NaCl and 50 U/mL heparin and stored at -80 °C. LPL mass was measured with a sandwich enzyme-linked immunoassay as described (22); LPL levels were calculated by linear regression from dilutions that fell within the linear range of the standard curve (from purified mouse LPL). LPL activity was measured with a [³H] triolein substrate using rat serum as a source of APOC2 (22). Activity was expressed as units of TG hydrolase activity (with 1 nM corresponding to 1 nmol fatty acid release/min).

Measuring Lipid Droplet Size in Brown Adipocytes. Mice were perfused with 20 mL PBS followed by 15 mL 2% PFA, 2.5% glutaraldehyde, and 2.1% sucrose in 0.1 M sodium cacodylate (pH 7.4). BAT was fixed in the same solution overnight at 4 °C. On the following day, tissues were processed for electron microscopy as described previously (38). Sections (500-nm-thick) were imaged using a Zeiss Supra 40VP scanning electron microscope set to 10 kV accelerating voltage and 5.5-mm WD using the backscatter detector. Representative images were captured, and individual adipocytes were numbered. Lipid droplet size was quantified with ImageJ (minimum of 130 brown adipocytes). The results from two trained observers were averaged, and the results expressed as the average lipid droplet area/cell.

Statistical Analyses. Data were analyzed with Prism 9 (GraphPad) and presented as mean \pm SEM (unless otherwise indicated). Statistical significance was

determined with an unpaired two-tailed Student's *t* test in studies involving two independent groups and one- or two-way ANOVA for studies involving multiple groups. A *P* value of less than 0.05 was considered significant.

Data, Materials, and Software Availability. The data have been deposited in a publicly accessible database (UCLA Dataverse: <https://doi.org/10.25346/S6/TQT2P>). Other study data are included in this article and *SI Appendix*.

ACKNOWLEDGMENTS. This work was supported from grants from the NHLBI (HL087228, HL146358, HL139725), an American Heart Association Grant Postdoctoral Fellowship (834131), a *Fondation Leducq* Transatlantic Network

Grant (19CVD04), a NOVO Nordisk Foundation Grant (NNF20OC0063444), and The John and Birthe Meyer Foundation.

Author affiliations: ^aDepartment of Medicine, David Geffen School of Medicine, University of California, Los Angeles, CA 90095; ^bFinsen Laboratory, Rigshospitalet DK-2200 Copenhagen N, Denmark; ^cBiotech Research and Innovation Centre, University of Copenhagen DK-220 Copenhagen N, Denmark; and ^dDepartment of Human Genetics, David Geffen School of Medicine, University of California, Los Angeles, CA 90095

Author contributions: W.S., A.P.B., S.G.Y., and L.G.F. designed research; W.S., Y.Y., P.H., Y.T., T.A.W., J.R.K., P.M., H.J., J.L.-C.F., C.T., A.P.B., and L.G.F. performed research; M.P., A.P.B., and L.G.F. contributed new reagents/analytic tools; W.S., A.P.B., and L.G.F. analyzed data; and W.S., S.G.Y., and L.G.F. wrote the paper.

1. S. G. Young *et al.*, A protein of capillary endothelial cells, GPIHBP1, is crucial for plasma triglyceride metabolism. *Proc. Natl. Acad. Sci. U.S.A.* **119**, e2211136119 (2022).
2. B. S. J. Davies *et al.*, GPIHBP1 is responsible for the entry of lipoprotein lipase into capillaries. *Cell Metab.* **12**, 42–52 (2010).
3. R. J. Havel, R. S. Gordon Jr., Idiopathic hyperlipemia: Metabolic studies in an affected family. *J. Clin. Invest.* **39**, 1777–1790 (1960).
4. A. P. Beigneux *et al.*, Chylomicronemia with a mutant GPIHBP1 (Q115P) that cannot bind lipoprotein lipase. *Arterioscler. Thromb. Vasc. Biol.* **29**, 956–962 (2009).
5. C. V. Voss *et al.*, Mutations in lipoprotein lipase that block binding to the endothelial cell transporter GPIHBP1. *Proc. Natl. Acad. Sci. U.S.A.* **108**, 7980–7984 (2011).
6. R. Franssen *et al.*, Chylomicronemia with low postheparin lipoprotein lipase levels in the setting of GPIHBP1 defects. *Circ. Cardiovasc. Genet.* **3**, 169–178 (2010).
7. S. Kersten, Physiological regulation of lipoprotein lipase. *Biochim. Biophys. Acta* **1841**, 919–933 (2014).
8. V. Sukonina, A. Lookene, T. Olivecrona, G. Olivecrona, Angiotensin-like protein 4 converts lipoprotein lipase to inactive monomers and modulates lipase activity in adipose tissue. *Proc. Natl. Acad. Sci. U.S.A.* **103**, 17450–17455 (2006).
9. K. Z. Leth-Espensen *et al.*, The intrinsic instability of the hydrolase domain of lipoprotein lipase facilitates its inactivation by ANGPTL4-catalyzed unfolding. *Proc. Natl. Acad. Sci. U.S.A.* **118**, e2026650118 (2021).
10. S. Mysling *et al.*, The angiotensin-like protein ANGPTL4 catalyzes unfolding of the hydrolase domain in lipoprotein lipase and the endothelial membrane protein GPIHBP1 counteracts this unfolding. *Elife* **5**, e20958 (2016).
11. K. K. Kristensen *et al.*, Unfolding of monomeric lipoprotein lipase by ANGPTL4: Insight into the regulation of plasma triglyceride metabolism. *Proc. Natl. Acad. Sci. U.S.A.* **117**, 4337–4346 (2020).
12. K. K. Kristensen, K. Z. Leth-Espensen, S. G. Young, M. Ploug, ANGPTL4 inactivates lipoprotein lipase by catalyzing the irreversible unfolding of LPL's hydrolase domain. *J. Lipid. Res.* **61**, 1253 (2020).
13. F. Oldoni *et al.*, ANGPTL8 has both endocrine and autocrine effects on substrate utilization. *JCI Insight* **5**, e138777 (2020).
14. J. F. Haller *et al.*, ANGPTL8 requires ANGPTL3 to inhibit lipoprotein lipase and plasma triglyceride clearance. *J. Lipid. Res.* **58**, 1166–1173 (2017).
15. Y. Wen, Y. Q. Chen, R. J. Konrad, The regulation of triacylglycerol metabolism and lipoprotein lipase activity. *Adv. Biol. (Weinheim)* **6**, e2200093 (2022), 10.1002/adbi.202200093.
16. M. Klingenspor, Cold-induced recruitment of brown adipose tissue thermogenesis. *Exp. Physiol.* **88**, 141–148 (2003).
17. A. Bartelt *et al.*, Brown adipose tissue activity controls triglyceride clearance. *Nat. Med.* **17**, 200–205 (2011).
18. W. Dijk *et al.*, ANGPTL4 mediates shuttling of lipid fuel to brown adipose tissue during sustained cold exposure. *Elife* **4**, e08428 (2015).
19. B. Cannon, J. Nedergaard, Nonshivering thermogenesis and its adequate measurement in metabolic studies. *J. Exp. Biol.* **214**, 242–253 (2011).
20. P. P. Khedoe *et al.*, Brown adipose tissue takes up plasma triglycerides mostly after lipolysis. *J. Lipid. Res.* **56**, 51–59 (2015).
21. A. M. Lund Winther, K. K. Kristensen, A. Kumari, M. Ploug, Expression and one-step purification of active LPL contemplated by biophysical considerations. *J. Lipid. Res.* **62**, 100149 (2021).
22. W. Song *et al.*, Electrostatic sheathing of lipoprotein lipase is essential for its movement across capillary endothelial cells. *J. Clin. Invest.* **132**, e157500 (2022).
23. B. S. Davies *et al.*, Assessing mechanisms of GPIHBP1 and lipoprotein lipase movement across endothelial cells. *J. Lipid. Res.* **53**, 2690–2697 (2012).
24. E. D. Korn, Clearing factor, a heparin-activated lipoprotein lipase. II. Substrate specificity and activation of coconut oil. *J. Biol. Chem.* **215**, 15–26 (1955).
25. E. D. Korn, Clearing factor, a heparin-activated lipoprotein lipase. I. Isolation and characterization of the enzyme from normal rat heart. *J. Biol. Chem.* **215**, 1–14 (1955).
26. A. J. Hoogwerf, L. A. Cisar, D. C. Evans, A. Bensadoun, Effect of chlorate on the sulfation of lipoprotein lipase and heparan sulfate proteoglycans. Sulfation of heparan sulfate proteoglycans affects lipoprotein lipase degradation. *J. Biol. Chem.* **266**, 16564–16571 (1991).
27. A. P. Beigneux *et al.*, Glycosylphosphatidylinositol-anchored high density lipoprotein-binding protein 1 plays a critical role in the lipolytic processing of chylomicrons. *Cell Metab.* **5**, 279–291 (2007).
28. A. P. Beigneux *et al.*, Highly conserved cysteines within the Ly6 domain of GPIHBP1 are crucial for the binding of lipoprotein lipase. *J. Biol. Chem.* **284**, 30240–30247 (2009).
29. A. P. Beigneux *et al.*, Assessing the role of the glycosylphosphatidylinositol-anchored high density lipoprotein-binding protein 1 (GPIHBP1) three-finger domain in binding lipoprotein lipase. *J. Biol. Chem.* **286**, 19735–19743 (2011).
30. M. M. Weinstein *et al.*, Abnormal patterns of lipoprotein lipase release into the plasma in GPIHBP1-deficient mice. *J. Biol. Chem.* **283**, 34511–34518 (2008).
31. C. N. Goulbourne *et al.*, The GPIHBP1-LPL complex is responsible for the margination of triglyceride-rich lipoproteins in capillaries. *Cell Metab.* **19**, 849–860 (2014).
32. W. Dijk *et al.*, Angiotensin-like 4 promotes intracellular degradation of lipoprotein lipase in adipocytes. *J. Lipid. Res.* **57**, 1670–1683 (2016).
33. W. Dijk, P. M. M. Ruppert, L. J. Oost, S. Kersten, Angiotensin-like 4 promotes the intracellular cleavage of lipoprotein lipase by PCSK3/furin in adipocytes. *J. Biol. Chem.* **293**, 14134–14145 (2018).
34. T. Olafsen *et al.*, Unexpected expression pattern for glycosylphosphatidylinositol-anchored HDL-binding protein 1 (GPIHBP1) in mouse tissues revealed by positron emission tomography scanning. *J. Biol. Chem.* **285**, 39239–39248 (2010).
35. C. He *et al.*, NanoSIMS analysis of intravascular lipolysis and lipid movement across capillaries and into cardiomyocytes. *Cell Metab.* **27**, 1055–1066.e3 (2018).
36. P. H. Weinstock *et al.*, Severe hypertriglyceridemia, reduced high density lipoprotein, and neonatal death in lipoprotein lipase knockout mice. Mild hypertriglyceridemia with impaired low density lipoprotein clearance in heterozygotes. *J. Clin. Invest.* **96**, 2555–2568 (1995).
37. K. J. Livak, T. D. Schmittgen, Analysis of relative gene expression data using real-time quantitative PCR and the 2^{-ΔΔC_T} method. *Methods* **25**, 402–408 (2001).
38. C. He *et al.*, High-resolution visualization and quantification of nucleic acid-based therapeutics in cells and tissues using Nanoscale secondary ion mass spectrometry (NanoSIMS). *Nucleic Acids Res.* **49**, 1–14 (2021).